Eur. Phys. J. B **46**, 315–324 (2005)
DOI: 10.1140/epjb/e2005-00261-9

THE EUROPEAN PHYSICAL JOURNAL B

Double exchange models: self consistent renormalisation

S. Kumar and P. Majumdar[a]

Harish-Chandra Research Institute, Chhatnag Road, Jhusi, Allahabad 211 019, India

Received 2 January 2005
Published online 18 August 2005 –

Abstract. We propose a scheme for constructing classical spin Hamiltonians from Hunds coupled spin-fermion models in the limit $J_H/t \to \infty$. The strong coupling between fermions and the core spins requires self-consistent calculation of the effective exchange in the model, either in the presence of inhomogeneities or with changing temperature. In this paper we establish the formalism and discuss results mainly on the "clean" double exchange model, with self consistently renormalised couplings, and compare our results with exact simulations. Our method allows access to system sizes much beyond the reach of exact simulations, and we can study transport and optical properties of the model without artificial broadening. The method discussed here forms the foundation of our papers [Phys. Rev. Lett. **91**, 246602 (2003), and Phys. Rev. Lett. **92**, 126602 (2004)].

PACS. 71.15.Pd Molecular dynamics calculations (Car-Parrinello) and other numerical simulations – 75.10.Hk Classical spin models – 72.15.-v Electronic conduction in metals and alloys

1 Introduction

The double exchange (DE) model was introduced by Zener [1] in 1951 to motivate ferromagnetism in the perovskite manganites. In contrast to 'Heisenberg like' coupling between localised spins, the effective interaction in 'double exchange' arises from optimisation of carrier kinetic energy in the spin background. The intimate correlation between spin configuration and electron motion had, till recently, restricted the study of the DE model to mostly qualitative analysis or mean field theory. The original proposal of Zener was followed up [2] by Anderson and Hasegawa, who clarified the physics of the coupled spin-fermion system in a two site model, and de Gennes [3] who presented a thermodynamic calculation and a phase diagram (incorporating antiferromagnetic superexchange). He produced the first estimate of transition temperature (T_c) in the model. The thermodynamic transition within double exchange was also studied [4] by Kubo and Ohata. This short list essentially exhausts activity on the double exchange problem prior to the 'manganite renaissance'.

The discovery of colossal magnetoresistance (CMR) and a variety of magnetic phases in the manganites [5] led to renewed interest in the DE model. In addition, the availability of powerful analytical and numerical tools, e.g., dynamical mean field theory (DMFT) and Monte Carlo methods provided impetus for studying the DE model in detail. In real systems the double exchange interaction is supplemented by [6] antiferromagnetic (AF) superexchange, electron-phonon interactions, and disorder, and some of these models have been studied within various approximations. The primary limitation of current methods, as we discuss in detail later, is their inability to access transport properties taking spatial fluctuations and disorder effects fully into account. In this context our method, of constructing an approximate but *explicit* classical spin Hamiltonian, allows a breakthrough. In the present paper our detailed results are on the simplest case, of the clean DE model. In earlier short publications we have presented results on the disordered double exchange model [7], and on magnetic phase competetion [8].

Let us define the general model to which our method is applicable. $H = H_{el} + H_{AF}$, with

$$H_{el} = \sum_{\langle ij\rangle,\sigma} t_{ij} c^{\dagger}_{i\sigma} c_{j\sigma} + \sum_i (\epsilon_i - \mu) n_i - J_H \sum_i \mathbf{S}_i.\vec{\sigma}_i$$
$$H_{AF} = J_S \sum_{\langle ij\rangle} \mathbf{S}_i \cdot \mathbf{S}_j. \qquad (1)$$

The $t_{ij} = -t$ are nearest neighbour hopping, on a square or cubic lattice as relevant. ϵ_i is the on site potential, uniformly distributed between $\pm\Delta/2$, say, and J_S is an antiferromagnetic superexchange between the core spins. J_H is the 'Hunds' coupling, and we will work in the limit $J_H/t \to \infty$. The parameters in the problem are Δ/t, J_S/t, and the carrier density n (or chemical potential μ). We assume a classical core spin, setting $|\mathbf{S}_i| = 1$, and absorb the magnitude of the spin in J_S. All our energy scales, frequency (ω) and temperature (T), etc., will be measured in units of t.

[a] e-mail: pinaki@mri.ernet.in

For $J_H/t \to \infty$ the fermion spin at a site is constrained to be parallel to the core spin, gaining energy $-J_H/2$, while the 'antiparallel' orientation is pushed to $+J_H/2$. Since the hopping term t_{ij} itself is spin conserving, the motion of the low energy, locally parallel spin, fermions is now controlled by nearest neighbour spin orientation. The strong magnetic coupling (J_H) generates an effective single band 'spinless fermion' problem [9], with core spin orientation dependent hopping amplitudes. We will discuss the hopping term further on, for the moment let us denote the renormalised (spin orientation dependent) hopping amplitude as $\tilde{t}$, indicative of double-exchange physics.

The $\tilde{t} - \Delta - J_S$ problem has a variety of ground states. (i) In the absence of J_S, both the 'clean' and the disordered DE model has a *ferromagnetic ground state*, at all electron density, with T_c reducing with increase in Δ. (ii) The non disordered problem, with J_S, leads to a variety of phases [10,11] competing with ferromagnetism. These are *ferromagnetic and A, C, G type AF phases*, etc. There could also be more exotic 'flux', 'skyrmion' or 'island' phases in some parts of parameter space. The boundaries between these phases are often first order so there are regimes of *macroscopic phase coexistence*. The specific set of possible AF phases depends on J_S. (iii) *Weak* disorder in the $\tilde{t} - J_S$ problem [8,12] converts the regions of macroscopic phase separation into *mesoscopic phase coexistence of FM and AF clusters.* (iv) For some density and $\Delta - J_S$ combination, the ground state could be a *spin glass*.

Although the phases above can be motivated easily, the electrical character of the ground state, or the temperature dependence of magnetic and transport properties, or the response to an applied magnetic field, are still not well understood. A comprehensive understanding of these effects within the relatively simple model in equation (1) would be the first step in approaching the even richer variety of phases in the manganites, where the lattice degrees of freedom are also active. This calls for a new technique, handling spatial and thermal fluctuations, the formation of clusters, and the effect of electron localisation. We propose and extensively benchmark such a real space technique in this paper. To appreciate the need for a new method let us quickly review the current approaches to the Hamiltonian above.

1.1 Theoretical approaches

The approaches can be broadly classified into three categories. These are: (i) Exact variational calculations [13] at $T = 0$, and generalisation [14–16] to $T \neq 0$ via approximate mean field techniques. Let us call these methods variational mean field (VMF), for convenience. (ii) Dynamical mean field theory (DMFT) based calculations [17,18] which map on the lattice model to an effective single site problem in a temporally fluctuating medium. Apart from a formal limit $d \to \infty$, where d is the number of spatial dimensions, there are no further approximations in the theory. (iii) Real space, finite size, Monte Carlo (MC) simulations [19–23] of the coupled 'spin-fermion' problem, treating the core spin as classical.

We can set a few indicators in terms of which the strength and weakness of various approximations can be judged. These are, tentatively:

1. The ability to access ground state properties.
2. Ability to handle fluctuations, and accuracy of T_c estimate.
3. The ability to access response functions, e.g., transport and optical properties.
4. Treatment of disorder effects: Anderson localisation and cluster coexistence.
5. Ability to handle Hubbard interactions, and quantum effects in spins and phonons.
6. Computational cost and finite size effects.

1.1.1 Variational calculations

The variational calculations attempt a minimisation of the energy of the (clean) system, at $T = 0$, with respect to a variety of ordered spin configurations. The optimal configuration $\{\mathbf{S}_i\}_{min}$ for specified J_S, μ, etc., is accepted as the magnetic ground state. The energy calculations are relatively straightforward, since the electron motion is in a periodic background. The method has been used to map out the ground state phase diagram of DE model with AF superexchange in two and three dimension [10,11]. The approach, however, can only be approximately implemented at finite temperature [14–16]. One has to calculate a spin distribution instead of just targeting the ground state, and estimating the energy of an electron system in a spin disordered background is non trivial. Due to the mean field character of VMF, fluctuation effects are lost and transition temperatures are somewhat overestimated. The method is focused on thermodynamic properties so there is no discussion of transport, etc, within this scheme (with one exception [14]). Disorder effects have been included, approximately [14], in some of these calculations. Variational methods can provide indication of phase coexistence [10,11] at $T = 0$, or, approximately, at finite temperature [15,16], but cluster coexistence in a disordered system is beyond its reach. The method has not been generalised to include quantum many body effects. Finite size effects in this approach are small and the method is relatively easy to implement.

1.1.2 Dynamical mean field theory

The single site nature of the DMFT approximation becomes exact in the limit of 'high dimensions'. DMFT can access both ground state and finite temperature properties, but the effective single site approximation cannot capture spatial fluctuations, or a non trivial paramagnetic phase. The 'mean field' character leads to an overestimate of T_c, and also the inability to differentiate between two and three dimensional systems. Being a Greens function based theory DMFT can readily access response functions.

However, effects like Anderson localisation or cluster coexistence, which require spatial information, cannot be accessed [24]. The method can handle many body, Hubbard like, interactions and quantum dynamics in all the variables involved, although such calculations are quite difficult. DMFT is defined directly in the thermodynamic limit, so there are no finite size effects. The calculations are relatively easy, when quantum many body effects are not involved, and have been a major tool in exploring phenomena in the manganites.

The limitations of DMFT become apparent as we consider the more complicated phases that can arise in our model. For instance in the strong disorder problem [7], when there is a possibility of electron localisation, the DMFT approach cannot access the insulating phase [24]. Neither can it access the spatially inhomogeneous nature of freezing, and the persistence of strong spin correlations above the bulk T_c. Similarly, in the problem of competing double exchange and superexchange, in the presence of weak disorder, the system breaks up into interspersed 'ferro-metallic' and 'AF-insulating' regions [8,12]. A complicated variant of this coexistence effect has been extensively studied in manganite experiments [25]. The 'single site' nature of DMFT cannot access cluster coexistence, except possibly in an averaged sense. The transport and metal-insulator transitions that can occur in this situation also remain inaccessible. So, there are important *qualitative effects* beyond the reach of DMFT, in systems where spatial inhomogeneity is important.

1.1.3 Monte Carlo

The finite size real space approach uses the Metropolis algorithm to generate equilibrium configurations of the spins at a given temperature. Monte Carlo calculations on classical systems with short range interactions involve a cost $\mathcal{O}(zN)$ for a system update, with z being the coordination number on the lattice and N the system size. In the spin-fermion problem, however, the 'cost' of a spin update at a site has to be computed from the fermion free energy. If one uses direct diagonalisation of the Hamiltonian to accomplish this, the cost *per site* is $\mathcal{O}(N^3)$, the cost for a 'system update' is a prohibitive N^4. All this is after ignoring quantum many body effects. Current MC approaches have not been generalised to handle Hubbard like interactions.

Despite the severe computational cost, this method, which we will call ED−MC (exact diagonalisation based MC), has been successfully used to clarify several aspects of manganite physics, and DE models in general. System sizes accessible are ∼100 at most (recent algorithms [22] have enhanced this somewhat), with 50−60 being more typical. This method can provide an outline of the finite temperature magnetic phase diagram, reveal major spectral features, and even yield the basic signatures of cluster coexistence. However, as is obvious from the accessible N, the finite size gaps are much too large for any reasonable estimate of d.c transport properties, and the small linear dimension available, in two or three spatial dimension, allows only a preliminary glimpse of coexistence physics. The size limitation apart, the method is *exact* and comprehensive, with none of the problems of standard quantum Monte Carlo (QMC). An extension of this approach to larger system sizes would allow exploration of several unresolved issues in manganite physics. Apart from the ED based MC, 'hybrid MC' results have been reported [11,23] for the various phases of double exchange competing with superexchange antiferromagnetism. No transport results, however, have yet been presented within this framework.

Our method, described in the next section, is developed in this spirit. It is a *real space Monte Carlo approach* with the key advantage that it avoids the iterative N^3 diagonalisation step. We extract an effective Hamiltonian for the core spins from the coupled spin-fermion problem, through a self-consistent scheme. We can work at arbitary temperature, handle strong disorder, and have better control on 'cluster physics' and transport properties due to our significantly larger system size, $N \sim 10^3$.

In the next section we describe our approximation and its computational implementation in detail. Following that we describe our results on the 'clean' DE model in two and three dimension. We will discuss results on thermodynamics, spectral features, resistivity and optical conductivity, in most of these cases, and compare with exact simulation results. We will also highlight systematically the size effects in transport and optical properties.

2 Method

2.1 The $J_H/t \to \infty$ limit

We have already written down our basic Hamiltonian in equation (1). The transformation and projection described in the next couple of paragraphs is well known, but we repeat them here for completeness.

Working at large J_H/t it is useful to 'diagonalise' the $J_H \mathbf{S}_i.\vec{\sigma}_i$ term first.The electron spin operator is $\vec{\sigma}_i = \sum_{\alpha\beta} c^\dagger_{i\alpha}\vec{\sigma}_{\alpha\beta}c_{i\beta}$, where the $\sigma^\mu_{\alpha\beta}$ are the Pauli matrices, and this 2×2 problem has eigenvalues $\pm J_H/2$. The eigenfunctions are linear combinations of the standard 'up' and 'down' z quantised fermion states at the site: $\gamma^\dagger_{i\mu} = \sum_\alpha A^i_{\mu\alpha}c^\dagger_{i\alpha}$. The lower energy state, $\gamma^\dagger_{il}$, a linear combination of the form $A^i_{11}c^\dagger_{i\uparrow} + A^i_{12}c^\dagger_{i\downarrow}$, is at energy $-J_H/2$ and has fermion spin parallel to the core spin $\mathbf{S}_i$. The orthogonal linear combination, $\gamma^\dagger_{iu}$, has fermion spin anti-parallel to the core spin and is at energy $+J_H/2$. The amplitudes $A^i_{\mu\alpha}$ are standard [9].

In the γ basis, the Hunds coupling term becomes $-(J_H/2)(\gamma^\dagger_{il}\gamma_{il} - \gamma^\dagger_{iu}\gamma_{iu})$ at all sites. The intersite hopping term, however, picks up a non trivial dependence on nearest neighbour spin orientation, $t_{ij}c^\dagger_{i\sigma}c_{i\sigma} \to \sum_{\alpha\beta} t_{ij}g^{\alpha\beta}_{ij}\gamma^\dagger_{i\alpha}\gamma_{j\beta}$ where α, β refer to the u, l indices. $g^{\alpha\beta}_{ij}$ arises from the product of the two transformations at site i and site j, and we will describe its specific form later. Since the canonical transformation is local, the density operator $\sum_\sigma c^\dagger_{i\sigma}c_{i\sigma} \to (\gamma^\dagger_{il}\gamma_{il} + \gamma^\dagger_{iu}\gamma_{iu})$.

At finite J_H/t this is just a transformation from the 'lab frame' to a local axis and the 'up' and 'down' spin fermions get mapped to (l,u), but we still have to solve a mixed 'two orbital problem'. However, if $J_H/t \to \infty$ then all the 'anti-parallel' $\gamma^\dagger_{iu}|0\rangle$ states get projected out and we can work solely in the subspace of states created by $\gamma^\dagger_{il}$. In this space, the Hamiltonian assumes a simpler form:

$$\begin{aligned} H_{el} &= -t\sum_{\langle ij\rangle}(g_{ij}\gamma^\dagger_i\gamma_j + \text{h.c.}) + \sum_i(\epsilon_i-\mu)n_i \\ &= -t\sum_{\langle ij\rangle} f_{ij}(e^{i\Phi_{ij}}\gamma^\dagger_i\gamma_j + \text{h.c.}) + \sum_i(\epsilon_i-\mu)n_i \quad (2) \end{aligned}$$

where we have dropped the superfluous ll label in g_{ij}, and absorbed $-J_H/2$ in the chemical potential. The hopping amplitude $g_{ij} = f_{ij}e^{i\Phi_{ij}}$ between locally aligned states, can be written in terms of the polar angle (θ_i) and azimuthal angle (ϕ_i) of the spin $\mathbf{S}_i$ as, $\cos\frac{\theta_i}{2}\cos\frac{\theta_j}{2} + \sin\frac{\theta_i}{2}\sin\frac{\theta_j}{2}e^{-i\ (\phi_i-\phi_j)}$. It is easily checked that the 'magnitude' of the overlap is $f_{ij} = \sqrt{(1+\mathbf{S}_i\cdot\mathbf{S}_j)/2}$, while the phase is specified by $\tan\Phi_{ij} = \text{Im}(g_{ij})/\text{Re}(g_{ij})$.

This problem can be viewed as a quadratic 'spinless fermion' problem with core spin dependent hopping amplitudes. The fermions move in the background of quenched disorder ϵ_i and 'annealed disorder' in the $\{\mathbf{S}_i\}$, where the second brackets indicate the full spin configuration. To exploit the nominally 'non interacting' structure of the fermion part we need to know the relevant spin configurations, $\{\mathbf{S}_i\}$, or, more generally, the distribution $P\{\mathbf{S}_i\}$, controlling the probability of occurence of a spin configuration.

2.2 Effective Hamiltonian for spins

The partition function of the system is $Z = \int \mathcal{D}\mathbf{S}_i \text{Tr}e^{-\beta H}$. To extract $P\{\mathbf{S}_i\}$ note that for a system with only spin degrees of freedom, Z will have the form $\int \mathcal{D}\mathbf{S}_i e^{-\beta H\{\mathbf{S}\}}$. Comparing this with the partition function of the spin-fermion problem we can use

$$\int \mathcal{D}\mathbf{S}_i \text{Tr}e^{-\beta H} \equiv \int \mathcal{D}\mathbf{S}_i e^{-\beta H_{\mathit{eff}}\{\mathbf{S}\}}$$

from which it follows that

$$\begin{aligned} H_{\mathit{eff}}\{\mathbf{S}_i\} &= -\frac{1}{\beta}\log\text{Tr}e^{-\beta H} \\ P\{\mathbf{S}_i\} &\propto e^{-H_{\mathit{eff}}\{\mathbf{S}_i\}}. \end{aligned} \quad (3)$$

The trace is over the fermion degrees of freedom. In our case

$$H_{\mathit{eff}} = -\frac{1}{\beta}\log\text{Tr}e^{-\beta H_{el}} + J_S\sum_{\langle ij\rangle}\mathbf{S}_i\cdot\mathbf{S}_j. \quad (4)$$

The principal difficulty in a simulation, and quite generally in spin-fermion problems, is in evaluating the first term on the r.h.s above for an *arbitrary spin configuration*. This is the origin of the N^3 factor in the exact MC. Our key proposal, whose analytic and numerical justification we provide later, is

$$-\frac{1}{\beta}\log\text{Tr}e^{-\beta H_{el}} \approx -\sum_{\langle ij\rangle} D_{ij}f_{ij} \quad (5)$$

where D_{ij} is an effective 'exchange constant' to be determined as follows. Define the operator $\hat{\Gamma}_{ij} = (e^{i\Phi_{ij}}\gamma^\dagger_i\gamma_j + \text{h.c.})$. This enters the 'hopping' part of the electron Hamiltonian. In any specified spin configuration $\{f,\Phi\}$ we can calculate the correlation function $D_{ij}\{f,\Phi\} = Z^{-1}_{el}\text{Tr}\hat{\Gamma}_{ij}e^{-\beta H_{el}}$, where Z_{el} is the electronic partition function in the specified background. The exchange that finally enters H_{eff} is the average of $D_{ij}\{f,\Phi\}$ over the assumed equilibrium distribution, i.e.: $D_{ij} = \int \mathcal{D}f\mathcal{D}\Phi P\{f,\Phi\}D_{ij}\{f,\Phi\}$ where we denote a spin configuration interchangeably by $\{f,\Phi\}$ or $\{\mathbf{S}\}$. Qualitatively, the 'effective exchange' is determined as the thermal average of a fermion correlator over the assumed equilibrium distribution. Let us bring together the equations for ready reference.

$$\begin{aligned} H_{el} &= -t\sum_{\langle ij\rangle} f_{ij}\hat{\Gamma}_{ij} + \sum_i(\epsilon_i-\mu)n_i \\ \hat{\Gamma}_{ij} &= (e^{i\Phi_{ij}}\gamma^\dagger_i\gamma_j + \text{h.c.}) \\ f_{ij} &= \sqrt{(1+\mathbf{S}_i\cdot\mathbf{S}_j)/2} \\ H_{\mathit{eff}}\{\mathbf{S}\} &= -\frac{1}{\beta}\log\text{Tr}e^{-\beta H_{el}} + J_S\sum_{\langle ij\rangle}\mathbf{S}_i\cdot\mathbf{S}_j \\ &\approx -\sum_{\langle ij\rangle} D_{ij}f_{ij} + J_S\sum_{\langle ij\rangle}\mathbf{S}_i\cdot\mathbf{S}_j \\ D_{ij} &= \langle\langle\hat{\Gamma}_{ij}\rangle\rangle_{H_{\mathit{eff}}}. \end{aligned} \quad (6)$$

The ED−MC approach 'solves' for physical properties by using the first four equations above: equilibriating the spin system by using H_{eff}, which itself involves a solution of the Schrödinger equation for the electrons.

Our method approximates the 'exact' H_{eff} by the form specified in the fifth equation and *computes an exchange*, rather than equilibrium configurations themselves, by fermion diagonalisation. The sixth equation indicates how the 'loop' is closed. We will refer to this method as "Self Consistent Renormalisation" (SCR) [26], or the H_{eff} scheme.

The nonlinear integral equation for the D_{ij} is solved to construct the 'classical spin model' for a set of electronic parameters, disorder realisation, and temperature. Although the assumption about H_{eff} seems 'obvious', and in fact something similar, but simpler, had been explored early on by Kubo and Ohata [4], and recently by Calderon and Brey [20], the power of the method becomes apparent in disordered systems or in the presence of competing interactions. In these cases the solutions D_{ij} can be spatially strongly inhomogeneous, and dramatically temperature dependent. The properties of such systems are far from obvious.

The equilibrium thermal average of any fermion operator, or correlation function, $\hat{O}$, can now be computed using the self-consistent distribution as:

$$\langle\langle \hat{O} \rangle\rangle = \int \mathcal{D}\{\mathbf{S}\} P\{\mathbf{S}\} O(\mathbf{S}). \tag{7}$$

The average $O(\mathbf{S})$ is computed on a spin configuration $\{\mathbf{S}_i\}$, with the configurations themselves picked according to the effective Boltzmann weight $\propto e^{-\beta H_{eff}}$.

We have not written the equation for μ. Since we would typically want to work at fixed density rather than fixed chemical potential, we employ the procedure above to calculate n and iterate μ till the 'target' density is obtained. In actual implementation, discussed later, the μ 'loop' and the D_{ij} 'loop' run simultaneously. We next discuss the analytic underpinning of our method before moving to numerical results.

2.3 Analytic limits

The central problem in DE models is construction of an energy functional for arbitrary spin configurations $\{f, \Phi\}$. This information is contained in the fermion free energy, $-T \log \mathrm{Tr} e^{-\beta H_{el}}$ as we have seen. We study two limits below, where the leading effects are well captured by our effective Hamiltonian.

2.3.1 Low temperature

If we ignore disorder and AF coupling, for simplicity, and if the free energy of the fermions can be approximated by the internal energy, then $D_{ij}\{f, \Phi\}$ contains the necessary information about the energy of *any spin configuration*: $\mathcal{E}\{f, \Phi\} \equiv H_{eff}\{f, \Phi\} = \sum_{ij} D_{ij}\{f, \Phi\} f_{ij}$. The *configuration dependent* correlation function, however, is hard to calculate, since it requires a solution of the Schrödinger equation for each spin configuration.

At low temperature, as the spins gradually randomise, the system explores configurations $\{f, \Phi\}$ near the ground state in the energy landscape. The relevant $D_{ij}\{f, \Phi\} \sim D^0_{ij} + \delta D_{ij}\{f, \Phi\}$, where D^0 is the 'exchange' computed on the ground state, and δD is the variation. At low T, such that the relevant $\delta D \ll D^0$, we can neglect the variation, δD, between configurations, and the 'effective Hamiltonian' assumes the form:

$$\begin{aligned} \lim_{T\to 0} H_{eff} &\sim -\sum_{\langle ij \rangle} D^0_{ij} f_{ij} \\ &= -\sum_{\langle ij \rangle} D^0_{ij} \sqrt{(1 + \mathbf{S}_i \cdot \mathbf{S}_j)/2}. \end{aligned}$$

As we will see in the simulations this approximation is remarkably good in the simple DE model almost upto $T_c/2$. At higher T the 'renormalisation' of D becomes important.

2.3.2 High temperature

For $T_c/T \ll 1$, cumulant expansion yields an asymptotically exact effective Hamiltonian:

$$H_{eff} \sim \lim_{\beta t \to 0} -\frac{1}{\beta} \ln \mathrm{Tr} \left(1 + \beta H + \frac{1}{2}\beta^2 H^2 + ...\right).$$

The leading contribution from this is:

$$H_{eff}^{high\ T} \sim -n(1-n)\beta t^2 \sum_{\langle ij \rangle} f_{ij}^2.$$

This apparently has a structure different from that of our H_{eff}, and additionally an 'effective coupling' falling off as $1/T$. In fact our coupling D has the same form, as can be checked by evaluating $\langle\langle \hat{\Gamma}_{ij} \rangle\rangle$ in a high temperature expansion. This quantity also depends on $n(1-n)$, to allow hopping, and falls off as $1/T$ since it is non local. The *self-consistent* calculation of the effective exchange, now based on the high temperature phase rather than the ground state, ensures that the leading contribution to the energy is well captured. The physical consequence of the $1/T$ effective exchange is that the susceptibility of the DE model does not have the Curie-Weiss form that one expects for Heisenberg like models [27].

The next order in series expansion will generate terms of the form:

$$\sum_{ijkl} f_{ij} f_{jk} f_{kl} f_{li} e^{i(\phi_{ij} + \phi_{jk} + ...)},$$

summed over the minimal plaquette. Higher powers in βt involve longer range excursion of the fermions, but the limited data available from exact simulations suggests that the critical properties of double exchange are similar to that of short range spin models.

Although the procedure above can be extended to extract an 'exact' effective Hamiltonian to high order in βt, we know of no such attempt. The only series expansion results available are on the $S = 1/2$ model, directly calculating thermodynamic properties [28].

2.4 Monte Carlo implementation

Since the ground state of the system is often not known it is usual to start from high temperature and follow the sequence below in generating the effective Hamiltonian and studying equilibrium properties.

(i) We start at high temperature, $T \gg T_c$, assuming some $D^n_{ij}(T)$, where n is the iteration index. and 'equilibriate' the system with this assumed effective Hamiltonian (not yet self-consistent). (ii) We compute the average $\langle\langle e^{i\Phi_{ij}} \gamma_i^\dagger \gamma_j + \mathrm{h.c.} \rangle\rangle$ over these (pseudo) equilibrium configurations. This generates $D^{n+1}_{ij}(T)$. (iii) Compare the generated exchange with the assumed exchange at each bond. Accept if within tolerance. If converged, then D_{ij} represents the correct 'exchange' at that temperature. Else, replace D^n_{ij} by D^{n+1}_{ij}. (iv) At each temperature and iteration, adjust μ as necessary to keep n constant.

At convergence fermion properties can be calculated and averaged over equilibrium MC configurations of the spin model. For a disordered system ($\Delta \neq 0$), the thermal cycle above has to be repeated for each realisation of disorder. In the clean problem, translation invariance forces the exchange to be uniform at all bonds, while $\Delta \neq 0$ generates a bond disordered spin model.

The computational effort needed in the ED−MC approach is $\propto N_{MC} \times N^4$, at each temperature, where N_{MC} is the number of MC sweeps (10^3−10^4), and N the size of the system (actually the Hilbert space dimension). As we have mentioned before, current resources allow $N_{max} \sim 100$. Within our H_{eff} scheme the MC configurations are generated using a short range spin model, with cost $\mathcal{O}(N)$. The actual cost is in determining the exchange: this is $\propto N_{iter} \times N_{av} \times N^3$, where N_{iter} is the number of iterations needed to get a converged solution, with ∼10% accuracy per bond, and N_{av} is the averaging needed *per iteration* for generating a reasonable 'equilibrium average'. Typically $N_{iter} \sim 4$ and $N_{av} \sim 50$.

We can roughly compare the computational cost of ED−MC with the H_{eff} scheme. For ED−MC, the time required is, $\tau_N \sim N_{MC} \times N^4$ at a given temperature. For the H_{eff} scheme, $\tau_N \sim N_{iter} \times N_{av} \times N^3$. Putting in the numbers, if resources allow $N \sim 100$ for the ED−MC approach, the same resource will allow $N \sim 1000$ within the H_{eff} scheme. In terms of computation time, H_{eff} is no more expensive than standard 'disorder average' in electronic systems.

2.5 Physical properties at equilibrium

The major physical properties we compute at equilibrium are optical conductivity and d.c resistivity, the density of states (DOS), and the magnetic structure factor.

(i) We estimate the d.c conductivity, σ_{dc}, by using the Kubo-Greenwood expression [29] for the optical conductivity. In a disordered non interacting system we have:

$$\sigma(\omega) = \frac{A}{N} \sum_{\alpha,\beta} (n_\alpha - n_\beta) \frac{|f_{\alpha\beta}|^2}{\epsilon_\beta - \epsilon_\alpha} \delta(\omega - (\epsilon_\beta - \epsilon_\alpha)). \quad (8)$$

The constant $A = (\pi e^2)/\hbar a_0$. The matrix element $f_{\alpha\beta} = \langle \psi_\alpha | j_x | \psi_\beta \rangle$ and we use the current operator $j_x = i a_0 \sum_{i,\sigma} (c^\dagger_{i+xa_0,\sigma} c_{i,\sigma} - \text{h.c.})$. The ψ_α etc. are single particle eigenstates, for a given equilibrium configuration, and $\epsilon_\alpha, \epsilon_\beta$ are the corresponding eigenvalues. The $n_\alpha = \theta(\mu - \epsilon_\alpha)$, etc., are occupation factors.

The conductivity above is prior to thermal or disorder averaging. Our simulations are in a square or cube geometry with periodic boundary condition. Given the finite size, the δ function constraint in $\sigma(\omega)$ cannot be satisfied for arbitrary ω. We use the following strategy: (i) calculate $\sigma_{int}(\omega) = \int_0^{\omega'} \sigma(\omega') d\omega'$, at three equispaced low frequency points, $\omega_1, \omega_2, \omega_3$, by summing over the delta functions in the appropriate range... (ii) thermally average the $\sigma_{int}(\omega)$ over the equilibrium configurations, (iii) invert: calculate a numerical derivative via three point interpolation, implementing $\bar{\sigma}(\omega) = d\bar{\sigma}_{int}(\omega)/d\omega$. The 'bar' on σ indicates thermal average. What we call the 'd.c. resistivity' is actually the inverse of a low frequency optical conductivity, computed by the method above. We systematically check the stability of our results by repeating the calculation for a sequence of system size (and reducing $\omega_1, \omega_2, \omega_3$ accordingly). For $N \sim 1000$, the 'd.c' conductivity is actually computed at $\omega \sim 0.06$.

Our transport calculation method and some benchmarks will be discussed in detail elsewhere [30]. To convert to 'real' units, note that our conductivity results are in units of $(\pi e^2)/\hbar a_0$. Since the Mott 'minimum' metallic conductivity, in three dimension, is $\sim (0.03 e^2/\hbar a_0)$, $\sigma = 1$ on our scale roughly corresponds to $10^2 \sigma_{Mott}$. The full $\sigma(\omega)$ is computed by computing $\sigma_{int}(\omega)$ defined above, thermal average, and inversion.

(ii) Each equilibrium magnetic configuration leads to a 'DOS' of the form $\sum_\alpha \delta(\omega - \epsilon_\alpha)$, where ϵ_α are the single particle eigenvalues in that background. The thermally averaged DOS that we show involves a Lorentzian broadening of each δ function, as indicated below.

$$N(\omega) \approx \frac{1}{N_{eq}} \sum_{eq} \sum_{\alpha} \frac{(\Gamma/\pi)}{(\omega - \epsilon_\alpha)^2 + \Gamma^2}. \quad (9)$$

The sum runs over the eigenvalues obtained in any spin configuration, and summed over equilibrium configurations. We use $\Gamma \sim 0.1$ in our results, although much smaller Γ would still give a smooth spectra at high T.

(iii) The magnetic structure factor is calculated as

$$S(\mathbf{Q}) = \frac{1}{N_{eq} N^2} \sum_{eq} \sum_{ij} \langle \mathbf{S}_i \cdot \mathbf{S}_j \rangle e^{i\mathbf{Q}\cdot(\mathbf{r}_i - \mathbf{r}_j)} \quad (10)$$

where i, j run over the entire lattice, and the outer average is over equilibrium configurations.

3 Results

In this section we provide a comprehensive comparison of results based on the 'exact' scheme (ED−MC) and our effective Hamiltonian approach, for the 'clean' DE model, and and extend the study to large sizes using the H_{eff} scheme. Most of our results are on three dimensional systems, where the simulations are more difficult and the results physically more relevant, and we show only limited data in two dimensions. The model is translation invariant, there are no competing interactions, and the low temperature phase is a ferromagnet.

3.1 Magnetism and thermodynamics

We begin with a comparison of the magnetisation, $m(T)$, obtained via ED-MC and SCR on 8×8 lattices in 2d, and 4^3 systems in 3d, with periodic boundary condition in all directions. Figure 1 compares the $m(T)$ obtained via the two schemes at three electron densities.

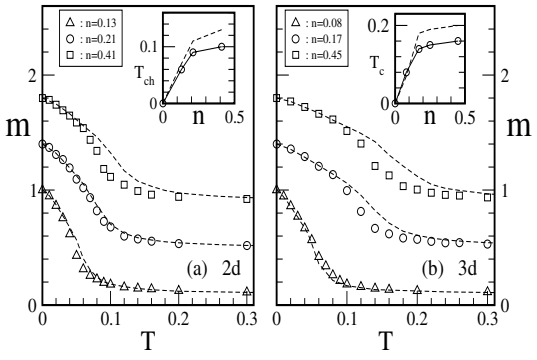

Fig. 1. Magnetism in 2d and 3d: open symbols are for ED−MC, the dotted lines indicate the SCR results, (a) 2d, (b) 3d. The insets show the T_c obtained via ED-MC (symbols) vs. SCR results (dotted lines).

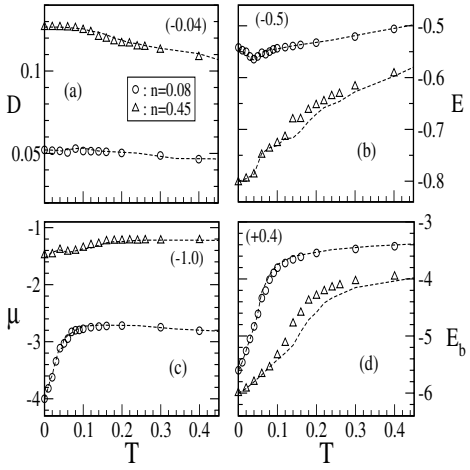

Fig. 2. Comparing thermodynamic indicators between ED-MC and the H_{eff} scheme in 3d: (a) effective exchange, (b) internal energy, (c) chemical potential and (d) band edge. Displayed value is actual value + shift. System size $4 \times 6 \times 4$. Open symbols: ED-MC, dotted lines: SCR.

Note at the outset that both the DE model and our H_{eff} are $O(3)$ symmetric and are *not* expected to have long range order at finite T in 2d (in an infinite system). However, as has been demonstrated in the case of the two dimensional classical Heisenberg model [31], $O(3)$ models have *exponentially large* correlation length at low temperature in 2d. For a nearest neighbour classical Heisenberg model with $|\mathbf{S}_i| = 1$, and exchange J, the low T correlation length $\xi(T) \sim 0.02e^{2\pi J/T}$. So, for $T \ll J$ even large finite lattices would look 'fully polarised' and one would need to access exponentially large sizes to see the destruction of long range order.

This allows us to define a (weakly size dependent) 'characteristic temperature' $T_{ch}(n)$ for the 2d DE model which marks the crossover from paramagnetic to a nominally 'ordered' phase. The true ordering temperature of strongly anisotropic DE systems, e.g., the layered manganites, which the planar model mimics, would be determined by the interplane coupling, but the in plane transport would be dictated mainly by the 2d fluctuations, as here.

The difference between ED-MC and SCR results in 2d, Figure 1a, is most prominent at the highest density, $n = 0.41$, where the T_{ch} inferred from these small size calculations differ by 15−20%. At lower density the difference is still visible but much smaller. We have indicated the T_{ch} scales inferred from the two schemes in the inset in Figure 1a. The difference between the two schemes is usually largest in clean high density systems, as we will see also in the three dimensional case. However, over the entire density range, the maximum deviation is ∼20%.

Notice that at all n, the low temperature $m(T)$ obtained via H_{eff} corresponds almost exactly with results based on ED−MC. This works upto $\sim T_{ch}/2$. The high temperature result within the two schemes is also in close correpondence but that is better illustrated in the thermodynamic data, Figure 2, which we will discuss later.

Figure 1b shows the results on magnetisation in the three dimensional problem at three densities, comparing results based on ED−MC and H_{eff}. As in two dimension the difference in the estimated T_c is greatest near the band center, being ∼15−20%, the correspondence improving as we move to $n \lesssim 0.2$. As before, the exact and approximate $m(T)$ match at low T for all densities.

Figure 2 which shows the thermodynamic indicators in the 3d case reveals that D_{ij} itself is virtually indistinguishable in the two schemes. The correlation $D_{ij} = \langle\langle \hat{I}_{ij} \rangle\rangle$ can be evaluated as an equilibrium average in an exact simulation also, although there it does not feed back into the calculation. The match between the D's computed in two different schemes, and across the density range, suggests that the difference in $m(T)$ seen near half-filling is not due to different numerical values of D, but the assumed *form* of H_{eff}. We either need a more sophisticated definition of the finite temperature D, or a different form of H_{eff} to bring the high density results of H_{eff} in closer correspondence with ED−MC. Notice that the D's are only weakly temperature dependent and the $m(T)$ at low temperature could have been obtained by setting $D(T) = D(0)$. In fact over the temperature range $0 - T_c$ the qualitative physics can be accessed without the thermal 'renormalisation' of the exchange. However, for $T \gg T_c$ the renormalisation is important, as suggested earlier by the high temperature expansion.

The results on all thermodynamic indicators, $D(T)$, $E(T)$, $\mu(T)$ and $E_b(T)$, Figure 2, show the close correspondence between results of the exact and approximate scheme. The D's are almost temperature independent in the range $0 - T_c$ and hardly distinguishable between ED−MC and H_{eff}, suggesting that effects beyond our effective Hamiltonian $-D\sum f_{ij}$ is needed to accurately describe the magnetic transition at the band center. The overall behaviour is similar in 2d as well so we are not presenting the 2d data.

We extend the H_{eff} scheme to large system size, and study the magnetism in 32^2 and 10^3 lattices. Figure 3 shows the results on $m(T)$, and the inset shows the T_c inferred from these simulations. The maximum T_c, occuring at band center is $\sim 0.2t$ which, with $t \sim (100-150)$ meV,

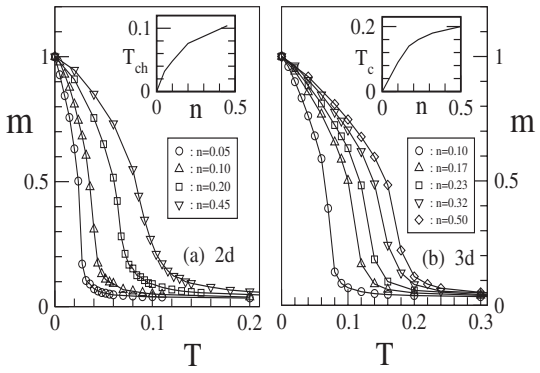

Fig. 3. Magnetisation based on H_{eff} in (a) 2d with 30×30 and (b) 3d with $10\times10\times10$ systems. Insets show the characteristic temperature scales inferred from $m(T)$.

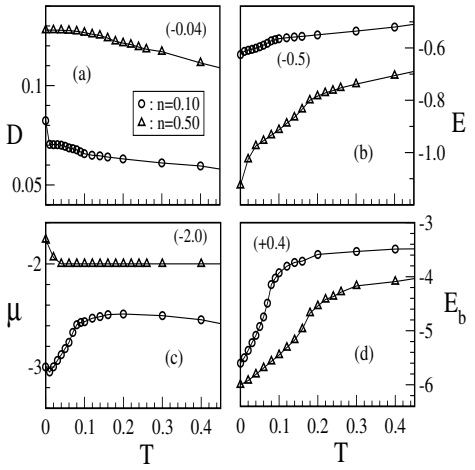

Fig. 4. Thermodynamic properties in the 3d case computed with H_{eff}, system size $N = 10\times10\times10$.

will be in the range $200-300$ K. These numbers are typical of high electron density Hunds coupled systems, and are in the right ballpark when compared to the manganites [32].

Figure 4 shows the thermodynamic indicators computed within the H_{eff} scheme on 10^3 in 3d. The strong temperature dependence in μ and E_b, seen also at small sizes, arise from the 'band narrowing' effect of spin disorder which reduces the mean hopping amplitude with increasing temperature.

3.2 Density of states

Figure 5 shows the density of states (DOS) computed at $n = 0.3$, four temperatures, and for a small, 4^3, and a large, 10^3, system. The mean level spacing at high temperature (where the spins are completely disordered) is $\sim12/L^3$ which is ~0.01 at $L = 10$ and ~0.18 at $L = 4$. For $T \to 0$, the polarised ferromagnetic state leads to large degeneracy and the level spacings could be more than 10 times larger than the high temperature value. We have broadened all δ functions by $\Gamma = 0.1$, so that the high temperature $L = 4$ spectra looks reasonable. With

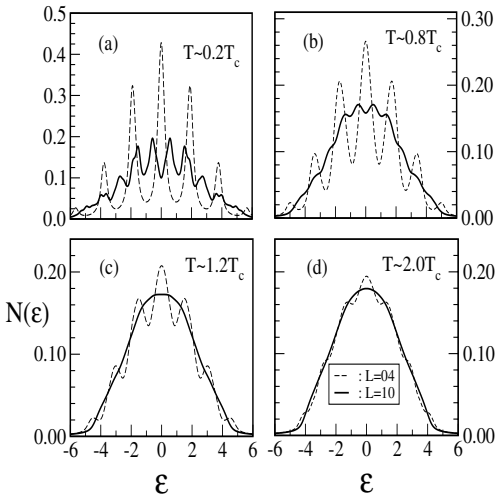

Fig. 5. DOS in three dimension. Results on H_{eff} with $4\times6\times4$ and $10\times10\times10$ geometry, $n = 0.3$.

this broadening the $L = 10$ data looks reasonable even below T_c.

This comparison highlights the unreliability of small size data in inferring spectral features over most of the interesting temperature range. Small sizes can often provide reasonable results on energetics, but on spectral features and, more importantly, on low frequency transport, they are completely unreliable.

3.3 Optical properties

Figure 6 shows the optical conductivity, $\sigma(\omega)$. The optical conductivity is a vital probe of charge dynamics in the system. Our data in the main panel, Figure 6, is for a $8\times8\times8$ geometry. At the lowest temperature there is an artificial 'hump' in $\sigma(\omega)$ which we think arises because the polarised three dimensional system has large degeneracy, and finite size effects are stronger than in two dimension. Nevertheless, there are some notable features in $\sigma(\omega)$, (i) the conductivity is Drude like, (ii) there is rapid reduction in low frequency spectral weight with increasing temperature, with some transfer to high frequency, (iii) the weight in $\sigma(\omega)$ is not conserved with increasing temperature, the loss is related to the suppression of kinetic energy with increasing spin disorder.

3.4 Resistivity

Finally, we look at the resistivity, which, surprisingly, has seen little discussion. Figure 7 shows the correlation between the ferromagnet to paramagnet transition and the rise in $\rho(T)$. We have normalised $\rho(T)$ in Figures 7a and 7b by the value at $T = 0.4$. The 'absolute' resistivity is shown in Figures 7c and 7d. Unlike mean field treatments which treat the paramagnetic phase as completely 'uncorrelated' and would yield a 'flat' resistivity for $T > T_{ch}$ (or T_c), there is a significant increase in $\rho(T)$ with rising temperature in the 'paramagnetic' phase as the short range spin

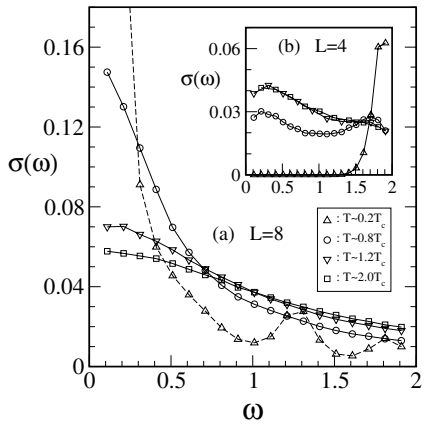

Fig. 6. Optical conductivity based on H_{eff} in three dimension. System size $4\times4\times4$ (inset) and $8\times8\times8$ (main panel), density $n = 0.3$. Symbols in the inset are same as in the main panel.

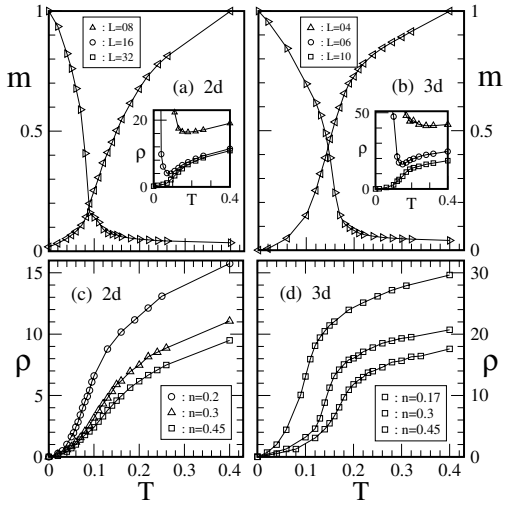

Fig. 7. (a, b) Magnetisation and normalised resistivity at $n = 0.3$ in (a) 2d and (b) 3d. Insets to (a) and (b) show the size dependence in the resistivity (see text). (c, d) Density dependence of $\rho(T)$, in 2d and 3d respectively, with system sizes 32×32 and (d) $10 \times 10 \times 10$.

correlation is gradually lost and the system heads towards the fully spin disordered phase. The general rise in $\rho(T)$ in the paramagnetic phase happens in both 2d and 3d, but surprisingly in 2d most of the rise seems to occur after the drop in $m(T)$, rather than across T_c as one sees in three dimension.

For a check on the reliability of the computed $\rho(T)$ the inset in Figure 7a shows the 'resistivity' computed on $L \times L$ geometry for $L = 8, 16, 32$ across the full temperature range. The $L = 8$ result has the same problem that we discussed in the context of $\sigma(\omega)$. The system essentially behaves as an 'insulator' at low T due to the finite size gap. The $L = 16$ data has similar upturn, but at a lower temperature. The data at $L = 24$ (not shown) and $L = 32$ are stable down to $T \sim 0.02$ and almost coincide, suggesting that except at very low temperature, results on these sizes are representative of bulk transport.

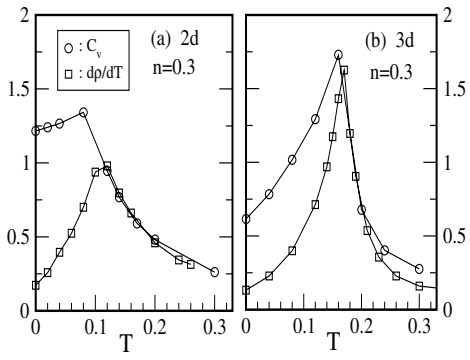

Fig. 8. Specific heat and $d\rho/dT$, at $n = 0.3$ in (a) 2d, and (b) 3d. System sizes used are same as in panels 7 (c, d).

The resistivity in the 3d case differs from 2d in that the major rise in $\rho(T)$ occurs around T_c in the 3d case, while it occurs *beyond* T_{ch} in the 2d case. Figure 7b shows $m(T)$ correlated with the normalised $\rho(T)$, and the rise is reminiscent of the Fisher-Langer result [33] in weak coupling electron-spin systems. The inset in Figure 7b shows the stability of the transport result in 3d for $L \gtrsim 8$, and the unreliability for $L \sim 4$.

Figures 7c and 7d, show the absolute resistivity for a few densities. The 'high temperature' 3d resistivity, at $T \sim 3T_c$ is approximately $15-25$, in the density range shown, which in real units would be $\sim(1-2)\,\mathrm{m}\Omega\,\mathrm{cm}$, roughly the high T resistivity of $La_{1-x}Sr_xMnO_3$ for $x \gtrsim 0.4$.

Figure 8 shows the correlation between $d\rho/dT$ and the specific heat in 2d and 3d. Above T_c and in 3d, panel (b), $d\rho/dT$ seems to match C_V very well, as expected from the perturbative results of Fisher and Langer [33]. In 2d however the correspondence is poor, probably due to incipient localisation effects in the resistivity. For $T \leq T_c$, even in 3d, the behaviours of C_V and $d\rho/dT$ are different because the rise in $m(T)$ affects the scattering rate, as is already known [33].

The validity of the 'weak coupling' results of Fisher-Langer, originally illustrated for a Heisenberg model, in this 'strong coupling' spin-fermion system may seem surprising. There are two reasons why the correspondence holds here: (i) the resistivity in the DE model arises from spin disorder induced weak fluctuations in the hopping amplitude, and is in the perturbative regime, and (ii) our magnetic model, H_{eff}, is effectively short range, and the critical properties of spin fluctuations are the same as in the Heisenberg model.

4 Conclusion

In this paper we proposed a new Monte Carlo technique that allows access to large system sizes but retains the correlated nature of spin fluctuations in the double exchange model. Combining this MC technique with a transport calculation based on the exact Kubo formula we presented a comprehensive solution of the model, including magnetism, thermodynamics, spectral features, transport, and optics.

This paper benchmarked the scheme for the clean double exchange model, where the complicated consistency and thermal renormalisation involved in the scheme are not crucial for a qualitative understanding. However, when we move to disordered systems [7], or non ferromagnetic ground states, or the regime of multiphase coexistence [8], the full power of a 'bond disordered' effective Hamiltonian, with non trivial spatial correlation between the bonds, becomes apparent.

For the clean ferromagnetic case one may try to improve the self-consistency scheme to obtain better correspondence [20,34] with ED−MC results. However, given the complexity of the current scheme, and the range of possibilities that it offers, we think it is more important to exploit the present scheme to resolve the outstanding *qualitative issues* first. Finally, although the entire scheme is presently implemented numerically, it would be useful to make analytic approximations within this framework to create greater qualitative understanding.

We acknowledge use of the Beowulf cluster at HRI.

References

1. C. Zener, Phys. Rev. **82**, 403 (1951)
2. P.W. Anderson, H. Hasegawa, Phys. Rev. **100**, 675 (1955)
3. P.G. de Gennes, Phys. Rev. **118**, 141 (1960)
4. K. Kubo, N. Ohata, J. Phys. Soc. Jpn **33**, 21 (1972)
5. A.P. Ramirez, J. Phys. Condens Matter **9**, 8171 (1997); E. Dagotto et al., Phys. Rep. **344**, 1 (2001), *Colossal Magnetoresistive Oxides*, edited by Y. Tokura (Gordon & Breach, 2000); M.B. Salamon, M. Jaime, Rev. Mod. Phys. **73**, 583 (2001)
6. See article by A.J. Millis, in *Colossal Magnetoresistive Oxides*, edited by Y. Tokura (Gordon & Breach, 2000)
7. S. Kumar, P. Majumdar, Phys. Rev. Lett. **91**, 246602 (2003)
8. S. Kumar, P. Majumdar, Phys. Rev. Lett. **92**, 126602 (2004)
9. E. Muller-Hartmann, E. Dagotto, Phys. Rev. B **54**, R6819 (1996)
10. H. Aliaga, B. Normand, K. Hallberg, M. Avignon, B. Alascio, Phys. Rev. B **64**, 024422 (2001)
11. J.L. Alonso, J.A. Capitan, L.A. Fernandez, F. Guinea, V. Martin-Mayor, Phys. Rev. B **64**, 054408 (2001)
12. A. Moreo, M. Mayr, A. Feiguin, S. Yunoki, E. Dagotto, Phys. Rev. Lett. **84**, 5568 (2000); J. Burgy, M. Mayr, V. Martin-Mayor, A. Moreo, E. Dagotto, Phys. Rev. Lett. **87**, 277202 (2001)
13. M. Yamanaka, W. Koshibae, S. Maekawa, Phys. Rev. Lett. **81**, 5604 (1998)
14. E.E. Narimanov, C.M. Varma, Phys. Rev. B **65**, 024429 (2002)
15. D.I. Golosov, Phys. Rev. B **58**, 8617 (1998)
16. J.L. Alonso, L.A. Fernandez, F. Guinea, V. Laliena, V. Martin-Mayor, Phys. Rev. B **63**, 064416 (2001)
17. N. Furukawa, J. Phys. Soc. Jpn **63**, 3214 (1995)
18. K. Nagai et al., J. Phys. Soc. Jpn **69**, 1837 (2000)
19. S. Yunoki, J. Hu, A.L. Malvezzi, A. Moreo, N. Furukawa, E. Dagotto, Phys. Rev. Lett. **80**, 845 (1998); E. Dagotto, S. Yunoki, A.L. Malvezzi, A. Moreo, J. Hu, Phys. Rev. B **58**, 6414 (1998)
20. M.J. Calderon, L. Brey, Phys. Rev. B **58**, 3286 (1998)
21. Y. Motome, N. Furukawa, J. Phys. Soc. Jpn **68**, 3853 (1999); J. Phys. Soc. Jpn **69**, 3785 (2000)
22. Y. Motome, N. Furukawa, J. Phys. Soc. Jpn **72**, 2126 (2003); Y. Motome, N. Furukawa, Phys. Rev. B **68**, 144432 (2003). The authors use an $\mathcal{O}(N)$ 'polynomial expansion' Monte Carlo technique to access large system sizes $\sim 16^3$. Unfortunately, there seems to be no benchmark or data on this method for systems involving magnetic phase competetion
23. J.L. Alonso et al., Nucl. Phys. B **596**, 587 (2001). The hybrid MC technique can apparently access sizes $\sim 16^3$, far beyond the reach of ED based techniques. However, there does not seem to be any follow up in disordered problems
24. DMFT cannot capture the quantum interference effects that lead to Anderson localisation. However, in the presence of strong *binary disorder* an insulating phase can arise due to a gap at the Fermi level, as for example in B.M. Letfulov, J.K. Freericks, Phys. Rev. B **64**, 174409 (2001); M. Auslender, E. Kagan, Phys. Rev. B **65**, 012408 (2001). This is unlike standard Anderson localisation where the disorder averaged density of states is finite even in the insulating phase
25. M. Uehara et al., Nature **399**, 560 (1999)
26. Our method should not be confused with the 'self-consistent renormalisation' scheme developed by T. Moriya and coworkers in the context of spin fluctuations in d electron systems
27. R.S. Fishman, M. Jarrell, Phys. Rev. B **67**, 100403(R) (2003)
28. H. Roder, R.R.P. Singh, J. Zang, Phys. Rev. B **56**, 5084 (1997).
29. see e.g., G.D. Mahan, *Many Particle Physics* (Plenum, New York, 1990)
30. S. Kumar, P. Majumdar, to be published
31. M. Takahashi, Phys. Rev. B **36**, 3791 (1987)
32. Comparing with results of other recent MC techniques, at $n = 0.5$ the $L \to \infty$ extrapolation of both hybrid MC [23] and polynomial expansion MC [22] give $T_c \sim 0.14t$. We do not have finite size scaling data but can guess that our $L \to \infty$ T_c will be $\sim 0.18t$
33. M.E. Fisher, J.S. Langer, Phys. Rev. Lett. **20**, 665 (1968)
34. I.V. Solovyev, Phys. Rev. B **67**, 014412 (2003)